ChemComm

Accepted Manuscript

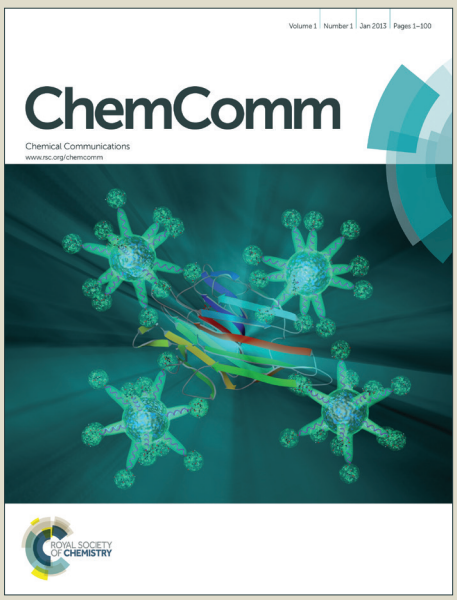

ROYAL SOCIETY OF CHEMISTRY

www.rsc.org/chemcomm

Journal Name

RSCPublishing

COMMUNICATION

Liquid-liquid interface-mediated room-temperature synthesis of amorphous NiCo pompoms from ultrathin nanosheets with high catalytic activity for hydrazine oxidation

Cite this: DOI: 10.1039/x0xx00000x

Received 00th January 2012,
Accepted 00th January 2012

DOI: 10.1039/x0xx00000x

www.rsc.org/

Hui Wang[1], Yanjiao Ma[1], Rongfang Wang[1,*], Julian Key[2], Vladimir Linkov[2] and Shan Ji[2,**]

Ni_xCo_y alloy pompoms formed by the aggregation of nano ultrathin sheets were prepared by simultaneous reduction of $NiCl_2$ and $CoCl_2$ with $NaBH_4$ via a liquid-liquid interface reaction. Ni_1Co_3 pompoms produced markedly higher activity and stability as hydrazine oxidation catalysts than Ni, Co and other Ni_xCo_y pompom catalysts.

Direct hydrazine (N_2H_4)-air fuel cells developed in the 1960s are highly attractive for high theoretical standard equilibrium potential (1.56 V), high power density (5400 W h L^{-1}), zero emission of CO_2, and absence of CO poisoning effects on electrocatalysts[1]. Hydrazine oxidation electrocatalysts have been under intensive study in recent years. Noble-metal catalysts such as platinum[2], palladium[3], gold[4], and silver[5] show good catalytic activity and stability for hydrazine oxidation, but their high cost and scarcity hinder the development of direct hydrazine-air fuel cells. Then, the search for efficient and stable non-noble-metal catalysts has attracted much research effort. Ni-based binary catalysts, such as Ni/MWNTs-textile[6], NiZn[7], NiCo[8], NiFe[9] and NiCu[10] etc.[11-13], offer promising hydrazine oxidation efficiency. It is well known that the shape, composition and size of metal nanocrystals are important parameters that determine the catalytic activity. Therefore, the architectural control of Ni-based alloy nanomaterials with well-defined shape affords another effective approach to improve hydrazine oxidation.

Recently, there have been an increasing number of excellent studies on novel nano/microstructural NiCo binary with various morphologies, such as tube arrays[14], wires[15], dumbbells[16], chains[17], flakes[18], flowers[19,20], needles[21] and sphere[22], synethesized by a polyol reduction[16,22], solvothermal method[17-19], electrodeposition[14], template-approach[16], and microemulsion system[21] technique. However, NiCo alloys with three-dimensional hierarchical nanostructures prepared via interfacial reactions have not been reported. Interfacial reactions have been used for guided growth of various nanostructures, such as NiSe[23], one-dimentional $Cu(OH)_2$[24], Au nanoleaves[25], PdNiP networks[26], charged Au nanocrystal monolayer[27], $NiCo_2O_4$ nanofilm[28], ordered Au, Pt and SiO_2 films[29], hollow ZnS and ZnO microspheres[30], and ZnO hollow-sphere nanofilm[31].

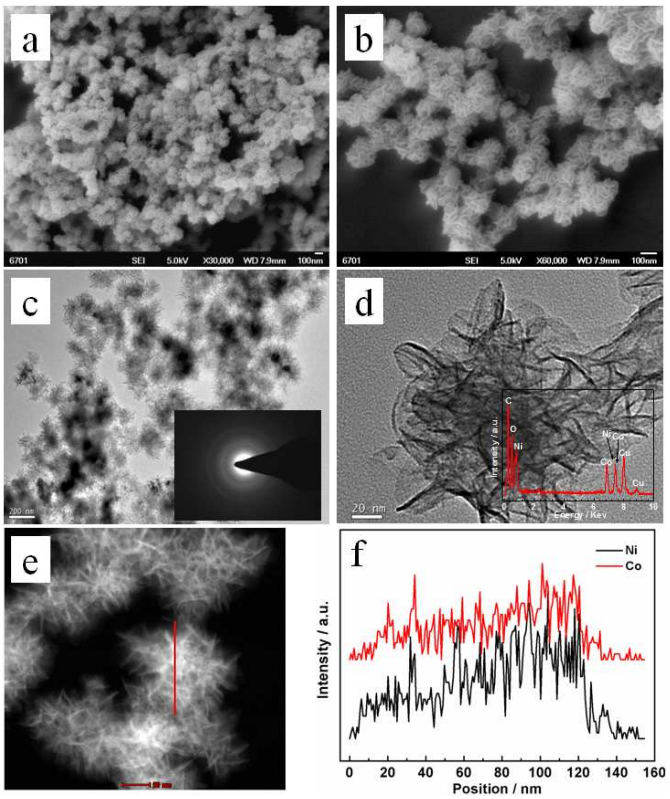

Figure 1. (a,b) SEM images, (c,d) TEM images of Ni_1Co_3 pompoms at different magnifications. The insets in c and d show its SAED pattern and EDX profile. (e) the STEM image and (f) line-scan EDX profiles of Ni_1Co_3 pompoms. The scale of the red line in the STEM images is consistent with that of the horizontal axis of the line-scan EDX profiles.

These products were formed by self-aggregation driven by the two-phase interface. Such results suggest that interfacial reactions could be used to synthesize NiCo alloys with unique structures. In this Communication, we report the interfacial synthesis of NiCo alloy ultrathin nanosheets in a two-phase system ($H_2O/CHCl_3$) that subsequently self-assemble to form pompoms-shaped particles driven by the water-in-oil interface. The as-synthesized NiCo alloy pompoms exhibited high hydrazine oxidation catalytic activity in alkaline medium.

Scanning electron microscopy (SEM) image in **Figure 1a** shows the overall morphology of Ni_1Co_3 pompoms, which reveals the obtained product comprised a large quantity of irregular spheres with diameters in the range of ca. 50-200 nm. The enlarged SEM image shown in Figure 1b indicates that the irregular spheres were aligned with each other and their surface consisted of fine curved nano-scale ridges, which was also characterized by transmission electron microscopy (TEM) shown in Figure 1c. High resolution TEM in Figure 1d shows that the pompoms comprised aggregated ultrathin sheets, and the ridges which formed the surface observed in the SEM images. The selected area electron diffraction pattern (inset Figure 1c) revealed a diffuse halo, indicating that Ni_1Co_3 had an amorphous state. Energy dispersive X-ray (EDX) analysis (inset Figure 1d) showed that the Co, Ni and O elements were present in the products, while C and Cu detection resulted from the presence of the carbon support membrane and copper net of the mounting stub. Figure 1e shows the scanning transmission electron microscopy (STEM) image of Ni_1Co_3 pompoms with the EDX line scan across a typical Ni_1Co_3 pompom. The intensity profile of Ni in Figure 1f concurrently overlapped with that of Co, suggesting that Ni and Co were evenly distributed throughout the Ni_1Co_3 pompoms, which was also demonstrated by the overlapping positions of the elemental mapping of Ni and Co displayed in Figure S1 in Supporting Information (ESI). Using ICP analysis (Table S1, ESI), the atomic ratio of Ni:Co in the bulk composition of Ni_1Co_3 pompoms was 1:3.02. The X-ray diffraction (XRD) pattern of Ni_1Co_3 pompoms (Figure S2, ESI) shows a broad weak peak ranging from $2\theta \approx 40$ to 50^0, suggesting Ni_1Co_3 is amorphous alloy, which is in accordance with the SAED result.

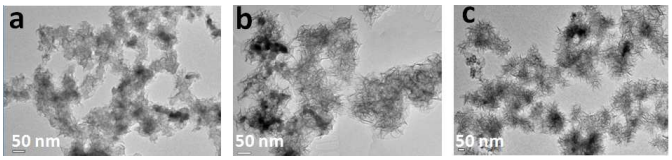

Figure 2. TEM images of Ni_1Co_3 pompoms collected at various times after the reaction occurs: (a) 2, (b) 4, (c) 6 h.

To have a complete view of the formation process of Ni_1Co_3 pompoms, a control experiment in the absence of one-phase, i.e. water, was first carried out. Here, micro-scale Ni_1Co_3 sheets were formed instead of a nano-structure (Figure S3, ESI). Therefore, we concluded that the two-phase interface played a key role in the formation of Ni_1Co_3 pompoms. At the same time, a morphological evolution study was conducted over an extended period of time. Products were collected from the reaction solution as a function of time, and their morphologies were observed by TEM. As shown in Figure 2, when the sample was collected after 2 h of reaction time, the product was composed of NiCo ultrasheets which overlapped in a disorderly fashion (Figure 2a). With prolonged reaction time, the aggregates began to form pompoms (Figure 2b), and finally, after 8 h, contiguous pompoms were formed in structures shown in Figure 2c.

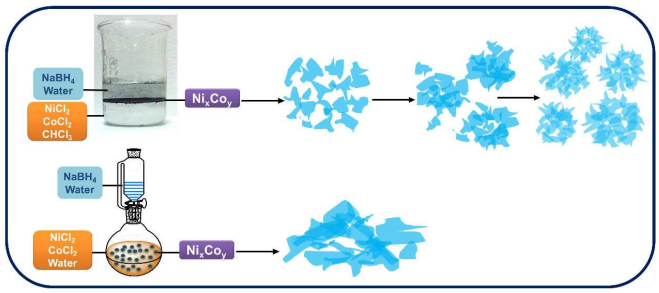

Scheme 1. Schematic process of Ni_1Co_3 pompoms formation in the interface region.

Based on the SEM and TEM results, a schematic illustration of the formation of Ni_1Co_3 pompoms is presented in Scheme 1. Firstly, Ni_1Co_3 small sheets are formed in solution through the co-reduction of Ni^{2+} and Co^{2+}. As the reaction continues, the formed nanosheets did not grow continually into micro-sheets like those formed in water solution, but tended to aggregate driven by the force of the interfaces[23]. Finally, the reaction results in nanosheets agglomerated continually, consequently, forming the pompom-like nanostructures. These pompoms could also agglomerate further, forming more complex hierarchical architectures. In addition, besides Ni_1Co_3 pompoms, a series of NiCo pompoms with various ratios, Ni, Ni_3Co_1, Ni_1Co_1, Ni_1Co_5, and Co could be successfully prepared by changing the molar ratio of metal precursors, as shown in Figure S4 and 5 (ESI). Thus, the composition of NiCo can be modulated by changing the molar ratio of the precursors while its amorphous structure and morphology can be remained.

Cyclic voltammograms (CVs) of Ni_xCo_y electrodes in 1.0 mol L^{-1} KOH were displayed in Figure 3a. The oxidation peaks on the positive scans of Ni (~0.26 V) and Co (~0.27 V) indicated the formation of higher-valent M (Co and Ni) surface oxygenates, e.g. M–OH or/and $M(OH)_2$, on the basis of the interaction of OH^- with the metal surface[11]. On the negative scan, reduction of the oxide occurred at about -0.05 V. For Ni_xCo_y alloys, the passivating effect of the surface metal hydroxide layer did not appear. All Ni_xCo_y alloys produced a featureless voltammetric response in KOH solution, suggesting they were electrochemically inactive in the potential window employed. The catalytic performance of all samples toward hydrazine oxidation was next evaluated by CVs in hydrazine hydrate solution. As seen in Figure 3b, an oxidation peak corresponding to hydrazine oxidation on all electrodes appeared in the forward scan, confirming that all materials were active for hydrazine oxidation; no hydrazine oxidation was observed during the reverse scan indicating the irreversible nature of the metal passivation.

Electrocatalytic hydrazine oxidation on the Ni electrode occurred at the potential of 0.016 V, rose, then dropped above 0.227 V. On the Co electrode, the onset potential of hydrazine oxidation is -0.04 V, and a maximum current density was achieved at 0.162 V. The negative shifts of the onset potential (56 mV) and peak potential (65 mV) of Co catalyst for hydrazine oxidation compared to those of Ni catalysts indicate that Co catalyst is more active than Ni catalyst for hydrazine oxidation.

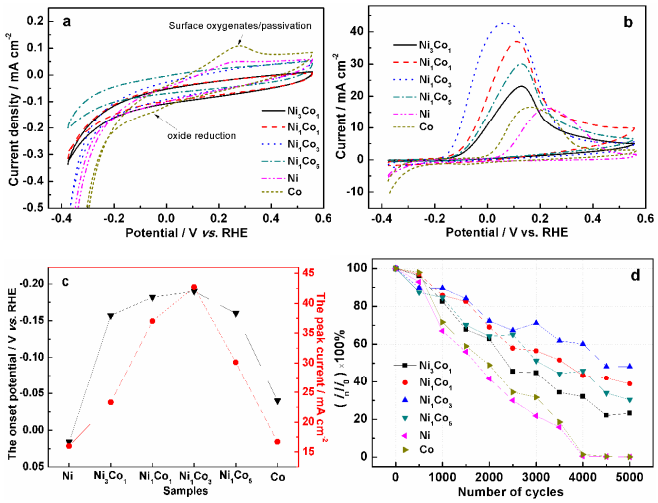

Figure 3. (a) CVs on Ni_3Co_1, Ni_1Co_1, Ni_1Co_3, Ni_1Co_5, Ni, and Co electrodes in 1.0 mol L^{-1} KOH solution at a scan rate of 20 mV s^{-1}. (b) CVs on Ni_3Co_1, Ni_1Co_1, Ni_1Co_3, Ni_1Co_5, Ni, and Co electrodes in 0.1 mol L^{-1} N_2H_4 + 1.0 mol L^{-1} KOH solution at a scan rate of 20 mV s^{-1}. (c) The onset potential and the oxidation peak current of all catalysts derived from Figure b. (d) The change of the oxidation peak current density related to the intial cycle with the increase of the cycles.

The result is similar to those given in previous reports by Asazawa et al.[32] and Sanabria-Chinchilla et al.[11]. For all Ni_xCo_y catalysts, the more negative onset potentials and higher peak currents than those of Ni and Co catalysts show that Ni_xCo_y pompoms have higher hydrazine oxidation catalytic activity due to the so-called liquid-phase electrochemical promotion effect of a chemical catalytic reaction (EPOC)[11]. The relation between the activity and the composition of Ni_xCo_y pompoms was express in Figure 3c in terms of the onset potential and the oxidation peak current of hydrazine oxidation. The catalytic activity of Ni_xCo_y pompoms presented a volcano curve, and reached a maximum when the Ni:Co atomic ratio was 1:3. As presented previously, the morphology and structure did not change from Ni_3Co_1 to Ni_1Co_5, suggesting these features were not related to the change of the catalytic activity. The specific surface area was considered to be the reason, since the large area would provide more active sites, and further result in an efficient catalytic process. Based on nitrogen adsorption isotherm at a relative pressure range between 0.02 and 0.26 shown in Figure S6 (ESI), the Brunauer-Emmett-Teller (BET) surface areas of Ni_3Co_1, Ni_1Co_1, Ni_1Co_3 and Ni_1Co_5 were 25.3, 36.5, 44.4, and 32.1 m^2 g^{-1} respectively. The trend is consistent with that of the catalytic activity, implying the BET surface area was the factor leading to different catalytic activities. In addition, the comparison with other Ni/Co/NiCo is displayed in Table S2 (ESI). As can be seen, the catalytic activity of Ni_1Co_3 pompoms was higher than that of $Ni_{0.5}Co_{0.5}$[8] and Co-CFC[33] in terms of the onset potential of hydrazine oxidation, and comparable to that of Ni/MWNTs-textile[6] in terms of the current of oxidation peak.

In order to investigate the reaction mechanism of hydrazine oxidation on Ni_1Co_3 electrode, CVs of hydrazine oxidation at different scan rates were performed. As shown in Figure S7a (ESI), with the increase of scan rate, the oxidation peak current (*I*p) of the hydrazine oxidation increased and the oxidation peak potential (*E*p) shifted slightly positively. Meanwhile, the *I*p increases linearly with the square root of the scan rate ($v^{1/2}$) in the range from 22 to 250 mV s^{-1} (Figure S7b, ESI), indicating a diffusion-controlled process rather than a surface controlled electron transfer kinetics[34]. Additionally, a linear relationship between *E*p and log(*v*) was also obtained (Figure S7c, ESI), demonstrating that hydrazine electrooxidation on Ni_1Co_3 was an irreversible process[35]. Based on the results, it is inferred that the overall electro-oxidation of hydrazine (i.e., $N_2H_4 + OH^- \rightarrow N_2 + H_2O + 4e^-$) occurred on Ni_1Co_3 electrode in alkaline solution.

To verify the stability of all as-prepared catalysts, all samples were subject to chronoamperometric and accelerated electrochemical degradation tests of repeating potential cycles. Chronoamperometric curves in Figure S8 (ESI) shows that Ni_1Co_3 possessed a higher current than other samples, and the current almost remained steady for continuous reaction of 1000 s. The decrease of catalytic activity was next evaluated by monitoring the residual of the oxidation peak current with the cycle number. As presented in Figure S9 (ESI), after 5000 cycles, the peak current for hydrazine oxidation on Ni_1Co_3 catalyst was retained ca.48% of the initial peak current, which was higher those of Ni_3Co_1 (23%), Ni_1Co_1 (39%), Ni_1Co_5 (30%), Ni (0.16%) and Co (0.2%) catalysts. The results indicated that the stability of Ni_1Co_3 was best among all the catalysts, maybe, due to EPOC effect and large BET surface area.

Conclusions

We have developed a facile procedure of a $CHCl_3$-H_2O liquid-liquid interface reaction to synthesize Ni_xCo_y alloy pompoms, which were assembled from ultrathin nanosheets driven by the force of the interface. The as-prepared Ni_xCo_y alloy pompoms can serve as efficient catalysts for hydrazine oxidation i.e. bearing higher oxidation peak current and lower onset potential than both Ni and Co catalysts. Optimum catalytic performance for hydrazine oxidation on Ni_xCo_y was achieved using a 1:3 atomic ratio composition of Ni:Co. Overall, Ni_1Co_3 pompoms appear to be a promising oxidation catalyst for direct hydrazine fuel cells. Moreover, our synthetic strategy reported herein could be extended to the rational design of other alloy nanomaterials with improved/unique functions through interface reaction.

This work was financially supported by the National Science Foundation of China (GrantNo. 21363022, 21163018, and 51362027).

Notes and references

[a] College of Chemistry and Chemical Engineering, Northwest Normal University, Lanzhou 730070, China
E-mail: wangrf@nwnu.edu.cn; Fax/Tel: +86 931 7971533

[b] South African Institute for Advanced Materials Chemistry, University of the Western Cape, Private Bag X17, Bellville, Cape Town 7535, South Africa
E-mail: sji@uwc.ac.za; Fax/Tel: +27-21-9599316

† Electronic Supplementary Information (ESI) available: [Experimental details, SEM, STEM, XRD, and Electrochemical performance of Ni_xCo_y]. See DOI: 10.1039/c000000x/

1. K. Asazawa, K. Yamada, H. Tanaka, A. Oka, M. Taniguchi and T. Kobayashi, *Angew. Chem. Int. Ed*., 2007, **46**, 8024-8027.
2. C. Roy, E. Bertin, M. H. Martin, S. Garbarino and D. Guay, *Electrocatalysis*, 2013, **4**, 76-84.
3. H. Lin, J. Yang, J. Liu, Y. Huang, J. Xiao and X. Zhang, *Electrochim. Acta*, 2013, **90**, 382-392.
4. M. G. Hosseini, M. M. Momeni and S. Zeynali, *Surf. Eng*., 2013, **29**, 65-69.
5. K. Ghanbari, *Synth. Met*., 2014, **195**, 234-240.
6. D. Zhang, B. Wang, D. Cao, K. Ye, Y. Xu, J. Yin, K. Cheng and G. Wang, *Mater. Sci. Eng. B*, 2014, **188**, 48-53.
7. U. Martinez, K. Asazawa, B. Halevi, A. Falase, B. Kiefer, A. Serov, M. Padilla, T. Olson, A. Datye, H. Tanaka and P. Atanassov, *Phys. Chem. Chem. Phys*. 2012, **14**, 5512-5517.
8. T. Sakamoto, K. Asazawa, K. Yamada and H. Tanaka, *Catal. Today*, 2011, **164**, 181-185.
9. J. Li, W. Tang, H. Yang, Z. Dong, J. Huang, S. Li, J. Wang, J. Jin and J. Ma, *RSC Adv*., 2014, **4**, 1988-1995.
10. B. Filanovsky, E. Granot, I. Presman, I. Kuras and F. Patolsky, *J. Power Sources*, 2014, **246**, 423-429.
11. J. Sanabria-Chinchilla, K. Asazawa, T. Sakamoto, K. Yamada, H. Tanaka and P. Strasser, *J. Am. Chem. Soc*., 2011, **133**, 5425-5431.
12. J. Li, W. Tang, J. Huang, J. Jin and J. Ma, *Catal. Sci. Technol*., 2013, **3**, 3155-3162.
13. J. Wang, Z. Dong, J. Huang, J. Li, X. Jin, J. Niu, J. Sun, J. Jin and J. Ma, *Appl. Surf. Sci*., 2013, **270**, 128-132.
14. X.-Z. Li, X.-W. Wei and Y. Ye, *Mater. Lett*., 2009, **63**, 578-580.
15. H. Jiang, J. Ma and C. Li, *Chem. Commun*., 2012, **48**, 4465-4467.
16. D. Ung, Y. Soumare, N. Chakroune, G. Viau, M. J. Vaulay, V. Richard and F. Fievet, *Chem. Mater*., 2007, **19**, 2084-2094.
17. L.-P. Zhu, H.-M. Xiao and S.-Y. Fu, *Eur. J. Inorg. Chem*., 2007, **25**, 3947-3951.
18. L. Zhang, S. Zhang, K. Zhang, G. Xu, X. He, S. Dong, Z. Liu, C. Huang, L. Gu and G. Cui, *Chem. Commun*., 2013, **49**, 3540-3542.
19. X.W. Wei, X.M. Zhou, K.L. Wu and Y. Chen, *CrystEngComm*, 2011, **13**, 1328.
20. I. Arief and P.K. Mukhopadhyay, *J. Magn. Magn. Mater*., 2014, **372**, 214-223.
21. D.E. Zhang, X.M. Ni, X.J. Zhang and H.-G. Zheng, *J. Magn. Magn. Mater*., 2006, **302**, 290-293.
22. P. Elumalai, H. N. Vasan, M. Verelst, P. Lecante, V. Carles and P. Taihades, *Mater. Res. Bull*., 2002, **37**, 353-363.
23. X. Wang, Q. Peng and Y. Li, *Acc. Chem. Res*., 2007, **40**, 635-643.
24. G. R. Bourret and R. B. Lennox, *J. Am. Chem. Soc*., 2010, **132**, 6657-6659.
25. S. Dutta, S. Sarkar, C. Ray, A. Roy, R. Sahoo and T. Pal, *ACS Appl. Mater. Interfaces* 2014, **6**, 9134-9143.
26. R. Wang, Y. Ma, H. Wang, K. Julian and S. Ji, *Chem. Commun*., 2014, **50**, 12877-12879.
27. F. Reincke, S.G. Hickey, W.K. Kegel and D. Vanmaekelbergh, *Angew. Chem. Int. Ed.*, 2004, **43**, 458-462.
28. L. Hu, L. Wu. M. Liao and X. Fang, *Adv. Mater*, 2011, **23**, 1988-1992.
29. Y.J. Li, W.J. Huang and S.G. Sun, *Angew. Chem. Int. Ed.*, 2006, **45**, 2537-2539.
30. L. Hu, M. Chen, W. Shan, T. Zhan, M. Liao X. Fang, X. Hu and L. Wu, *Adv. Mater*, 2012, **24**, 5872-5877.
31. M. Chen, L. Hu, J. Xu, M. Liao, L. Wu and X. Fang, *Small*, 2011, **7**, 2449-2453.
32. K. Asazawa, K. Yamada, H. Tanaka, M. Taniguchi and K. Oguro, *J. Power Sources*, 2009, **191**, 362-365.
33. R. Liu, X. Jiang, F. Guo, N. Shi, J. Yin, G. Wang and D. Cao, *Electrochim. Acta*, 2013, **94**, 214-218.
34. Y. Liang, Y. Zhou, J. Ma, J. Zhao, Y. Chen, Y. Tang and T. Lu, *Appl. Catal. B*, 2011, **103**, 388-396.
35. Y. Liang, K. Wu, C. Ge, Y. Zhou, Y. Chen, Y. Tang and T. Lu, *Fuel Cells*, 2012, **12**, 946-955.

